NEURODEVELOPMENT

Release of stem cells from quiescence reveals gliogenic domains in the adult mouse brain

Ana C. Delgado[1], Angel R. Maldonado-Soto[2], Violeta Silva-Vargas[1], Dogukan Mizrak[3,4]†, Thomas von Känel[1], Kelly R. Tan[1], Alex Paul[5]‡, Aviv Madar[6]§, Henar Cuervo[7], Jan Kitajewski[7], Chyuan-Sheng Lin[3,8], Fiona Doetsch[1]*

Quiescent neural stem cells (NSCs) in the adult mouse ventricular-subventricular zone (V-SVZ) undergo activation to generate neurons and some glia. Here we show that platelet-derived growth factor receptor beta (PDGFRβ) is expressed by adult V-SVZ NSCs that generate olfactory bulb interneurons and glia. Selective deletion of PDGFRβ in adult V-SVZ NSCs leads to their release from quiescence, uncovering gliogenic domains for different glial cell types. These domains are also recruited upon injury. We identify an intraventricular oligodendrocyte progenitor derived from NSCs inside the brain ventricles that contacts supraependymal axons. Together, our findings reveal that the adult V-SVZ contains spatial domains for gliogenesis, in addition to those for neurogenesis. These gliogenic NSC domains tend to be quiescent under homeostasis and may contribute to brain plasticity.

Neural stem cells (NSCs) in the adult mouse ventricular-subventricular zone (V-SVZ) have a regional identity and, depending on their spatial location, give rise to different subtypes of olfactory bulb interneurons (*1*). The adult V-SVZ also generates low numbers of glia under baseline conditions, but whether multiple gliogenic domains exist in the V-SVZ is unknown.

The V-SVZ extends along the lateral ventricles, along both the lateral wall, adjacent to the striatum, and the septal wall, adjacent to the septum, which is far less studied (Fig. 1A and fig. S1D). V-SVZ NSCs are largely quiescent, and both intrinsic and extrinsic signals actively maintain this state. To uncover potential regulators of adult V-SVZ NSC quiescence, we compared the transcriptomes of purified quiescent and activated adult V-SVZ NSCs (*2*) and identified platelet-derived growth factor beta (PDGFRβ), a tyrosine kinase receptor, as highly enriched in quiescent adult V-SVZ NSCs (qNSCs).

To characterize PDGFRβ expression in vivo in the V-SVZ, we performed immunostaining with lineage markers. Adult NSCs are radial $GFAP^+$ cells (GFAP, glial fibrillary acidic protein) (*2*, *3*) that contact the ventricle at the center of pinwheels formed by ependymal cells (*4*) and have a primary cilium (*5*). In whole-mount preparations, PDGFRβ was expressed by NSCs at the center of pinwheels throughout the rostral-caudal extent of the ventricle (Fig. 1B and fig. S1, A, B, and E), with their typical radial morphology revealed by electroporation of a PDGFRβ::mCherry reporter plasmid (Fig. 1C). About 95% of $GFAP^+$ V-SVZ cells expressed PDGFRβ (fig. S1, H and L). As NSCs become activated, they up-regulate epidermal growth factor receptor (EGFR). PDGFRβ was expressed in ~50% of activated NSCs (aNSCs; $GFAP^+EGFR^+$), corresponding to ~2.5% of $GFAP^+$ V-SVZ cells all of which expressed low levels of EGFR (Fig. 1D and fig. S1, I and M), but not in late aNSCs with high levels of EGFR, transit-amplifying cells (TACs; $GFAP^-EGFR^+$), or doublecortin (DCX^+) neuroblasts (Fig. 1D and fig. S1, J, K, and N). PDGFRβ was expressed in $CD13^+$ pericytes throughout the brain (fig. S1, C and F) and in some parenchymal astrocytes (*6*). We did not detect PDGFRβ in $Olig2^+$ oligodendrocytes (fig. S1O) or $NeuN^+$ neurons near the V-SVZ. Therefore, within the V-SVZ lineage, PDGFRβ is expressed in adult V-SVZ NSCs, which are largely quiescent.

$PDGFR\beta^+$ V-SVZ cells were long-term neurogenic and gliogenic in vivo, as shown by lineage tracing using PDGFRβ-P2A-$CreER^{T2}$; mT/mG mice (fig. S2A). Thirty and 120 days after tamoxifen injection, increasing numbers of GFP^+ immature DCX^+ (GFP, green fluorescent protein) and mature $NeuN^+$ neurons were detected in the olfactory bulb, and GFP^+Olig2^+ oligodendrocytes in the corpus callosum (Fig. 1E and fig. S2, B to F). Within the V-SVZ, GFP^+GFAP^+ radial cells, TACs, and migrating neuroblasts (Fig. 1F and fig. S2, G to I) were still present at both time points, revealing that $PDGFR\beta^+$ V-SVZ stem cells generate progeny 4 months after induction.

To assess the molecular and functional properties of $PDGFR\beta^+$ NSCs, we FACS-purified them from GFAP::GFP mice (FACS, fluorescence-activated cell sorting). The vast majority of $GFP^+PDGFR\beta^+$ cells were EGFR negative and corresponded to our previously described $CD133^+$ and $CD133^-GFP^+$ populations ($P\beta^+CD133^+$ and $P\beta^+$, respectively) (Fig. 1G) (*2*). As seen by immunostaining, PDGFRβ resolved the $EGFR^+$ aNSCs into two populations: $P\beta^+EGFR^+$ and $P\beta^-EGFR^+$ (Fig. 1G). RNA sequencing (RNA-seq) and functional analysis revealed that expression of PDGFRβ was inversely correlated with EGFR expression and cell division (fig. S2J). The kinetics of colony formation reflected expression of PDGFRβ, with $P\beta^+EGFR^-$ populations having slower kinetics than $EGFR^+$ populations, and the $P\beta^+EGFR^+$ population in between them (Fig. 1H and fig. S2K). Upon differentiation, all populations were multipotent (fig. S2L). Genome-wide correlation analysis showed that $P\beta^+EGFR^+$ cells had intermediate correlation scores, between those of $P\beta^+$-only and $P\beta^-EGFR^+$ populations, whereas $P\beta^+$-only populations were similar to each other and to cortical astrocytes (Fig. 1I). Finally, molecular comparisons of qNSCs to the $P\beta^+EGFR^+$ population highlighted known (*2*, *7*) and novel Gene Ontology quiescence pathways (fig. S2M and tables S1 to S3). In contrast, pathways including those related to entry into the cell cycle and regulation of translation initiation were enriched in $P\beta^+EGFR^+$ cells (fig. S2N). Consistent with their faster in vitro activation kinetics, most of the pathways enriched in $P\beta^-EGFR^+$ versus $P\beta^+EGFR^+$ cells were cell cycle and cytoskeletal remodeling related (fig. S2, O and P).

To functionally assess the effect of deleting PDGFRβ selectively in adult $GFAP^+$ V-SVZ NSCs in vivo, we generated inducible triple transgenic hGFAP::$CreER^{T2}$;$PDGFR\beta^{+/+}$;A14 ($PDGFR\beta^{WT}$) and mutant hGFAP::$CreER^{T2}$;$PDGFR\beta^{fl/fl}$;A14 ($PDGFR\beta^{\Delta}$) mice in which $CreER^{T2}$ recombinase is under the control of the human GFAP promoter (hGFAP::$CreER^{T2}$). Upon tamoxifen injection, the first and second immunoglobulin domains of the *pdgfrb* gene are deleted, preventing PDGF-ligand binding (*8*), and tdTomato is expressed, allowing cell fate to be followed (fig. S3A). Phosphorylation of PDGFRβ was greatly reduced in Tom^+ radial stem cells in $PDGFR\beta^{\Delta}$ mice (fig. S3B). Deletion of PDGFRβ led to an increase in activated stem cells and dividing stem cells 1 day after ending tamoxifen injections (1 dpi) (Fig. 2, A to D). TACs and neuroblasts were also increased (Fig. 2A and fig. S3, C and D). We also detected a small increase in $Tom^+Caspase3^+$ cells in $PDGFR\beta^{\Delta}$ mice, consistent with a role for PDGFRβ in cell survival in other cell types (*9*) (fig. S3, E and F), but their proportion was very low compared with the large increase in total Tom^+ cell number. The increased activation of NSCs in $PDGFR\beta^{\Delta}$

[1]Biozentrum, University of Basel, Basel, Switzerland. [2]Department of Neurology, Columbia University, New York, NY, USA. [3]Department of Pathology and Cell Biology, Columbia University, New York, NY, USA. [4]Department of Systems Biology, Columbia University, New York, NY, USA. [5]Department of Genetics and Development, Columbia University, New York, NY, USA. [6]Department of Biology, Center for Genomics and Systems Biology, New York University, New York, NY, USA. [7]Department of Physiology and Biophysics, University of Illinois at Chicago, Chicago, IL, USA. [8]Herbert Irving Comprehensive Cancer Center, Columbia University Medical Center, New York, NY, USA.
*Corresponding author. Email: fiona.doetsch@unibas.ch
†Present address: Department of Cardiac Surgery, University of Michigan, Ann Arbor, MI, USA. ‡Present address: Laboratory of Social Evolution and Behavior, Rockefeller University, New York, NY, USA. §Present address: Valo Health, Boston, MA, USA.

mice resulted in more mature neurons in the olfactory bulb (Fig. 2, E and F) and more oligodendrocytes in the corpus callosum than in control mice at 45 and 180 dpi (Fig. 2, G and H). Stem cell activation and progeny remained increased at later time points in the V-SVZ (fig. S3, G to I).

Adult NSCs contact the ventricle and are bathed by cerebrospinal fluid. Platelet-derived growth factor D (PDGFDD) ligand, which binds specifically to PDGFRβ, was detected by enzyme-linked immunosorbent assay (ELISA) in both the cerebrospinal fluid and the choroid plexus, a key source of secreted factors in the cerebrospinal fluid (*10*) (fig. S3J). To independently confirm that blocking PDGFRβ signaling promotes qNSC activation, we cultured FACS-purified qNSCs with PDGFDD ligand and PDGFRβ-blocking antibodies. Again, more qNSCs became activated to give rise to colonies, and with faster activation kinetics, than did isotype controls (Fig. 2, I and J).

PDGFRβ is therefore expressed in qNSCs in the adult V-SVZ, and is down-regulated as stem cells activate. Indeed, deletion of PDGFRβ selectively in adult NSCs releases them from quiescence, in contrast to deleting PDGFRβ embryonically (*11*, *12*). As such, PDGFRβ likely exerts distinct functions at different stages of brain development and in different cell types, such as pericytes (*13*, *14*).

The release of adult NSCs from quiescence in PDGFRβ$^{\Delta}$ mice provides a powerful tool to uncover V-SVZ NSC domains in vivo that are normally more quiescent. In the adult V-SVZ, olfactory bulb interneurons arise from throughout the lateral wall and rostral levels of the septal wall, and oligodendrocytes from the dorsal-lateral V-SVZ (*1*, *15*). PDGFRβ$^{\Delta}$ mice revealed both unknown glial cell types and several gliogenic domains in the adult V-SVZ, which are less proliferative under homeostasis.

Several types of GFAP^{+} cells with different distributions and morphologies in the V-SVZ were present in both wild-type and PDGFRβ$^{\Delta}$ mice. Radial GFAP^{+} cells with a process perpendicular to the ventricle were present in both lateral and septal walls but were more enriched in the dorsal and ventral V-SVZ (Fig. 3, A and B, and fig. S4A). A second radial GFAP^{+} cell with a process parallel to the ventricle was more prevalent on the septal side (Fig. 3, A and B, and fig. S4B). At 1 dpi, both were significantly increased (Fig. 3C).

We identified an astrocytic cell type, which we named gorditas, with a rounded soma with short GFAP^{+} processes (Fig. 3, A and B, and fig. S4C), enriched in the septal side and rare in wild-type mice. In contrast to mature stellate parenchymal astrocytes, which express low levels of GFAP (fig. S4D) and have a highly branched and bushy morphology, gorditas were strongly GFAP^{+}, had smaller soma and nuclei (fig. S4, E, F, and H), and had fewer primary processes (fig. S4, G, H, and K). About 70% expressed dim nestin (fig. S4I), and they were rarely MCM2^{+} in either control or PDGFRβ$^{\Delta}$ mice. Gorditas were most prevalent adjacent to the midventral septal wall from rostral to mid levels (Bregma +1.25 to +0.5 mm) of the V-SVZ (fig. S4, J, L, and M), and were significantly increased only in this septal domain of PDGFRβ$^{\Delta}$ mice (Fig. 3C and fig. S4J), at both 1 and 45 dpi (Fig. 3D). Tom^{+} mature stellate astrocytes were also increased in the septum (fig. S4, M and N) but not in the striatum or cortex (fig. S4O) at 45 dpi in PDGFRβ$^{\Delta}$ mice. Together, these findings highlight the diversity of astrocytes in the septal region.

The release from quiescence also uncovered multiple oligodendrogenic domains. We mapped their distribution by quantifying Tom^{+}Olig2^{+} cells in different subregions of the V-SVZ at 1 dpi (Fig. 3E and fig. S5, A to F). The dorsolateral wedge, known to be oligodendrogenic (*15*), and corpus callosum had increased Tom^{+}Olig2^{+} cells in PDGFRβ$^{\Delta}$ mice (fig. S5, A and B). Overall, the septal wall contained more Tom^{+}Olig2^{+}MCM2^{+} cells than did the lateral wall (Fig. 3G and fig. S5, F and G), with a focal

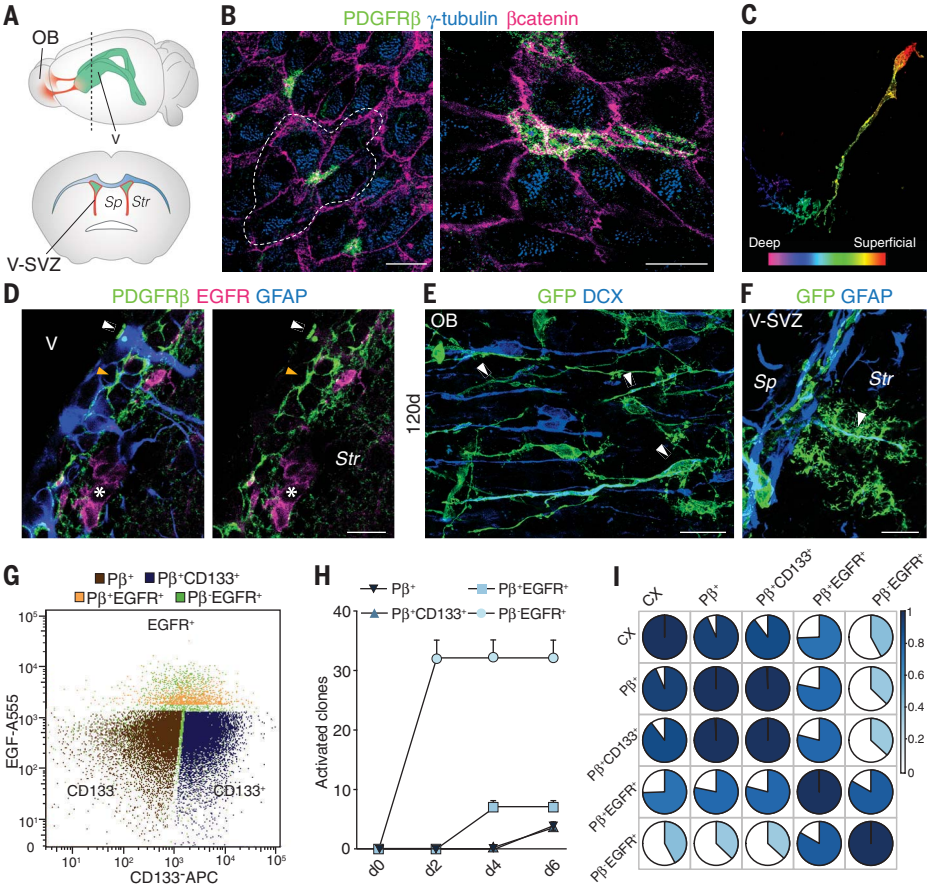

Fig. 1. PDGFRβ is expressed by adult V-SVZ NSCs. (**A**) Schema of whole mouse brain (top) and coronal section (bottom) at the level of the dashed line. The V-SVZ is adjacent to the lateral ventricles (V, green) and generates neurons that migrate to the olfactory bulb (OB). Sp, septum; Str; striatum. (**B**) Whole mounts showing clusters of PDGFRβ^{+} NSCs (green) at the center of ependymal cell pinwheels (dashed line shows one pinwheel). (**C**) Radial morphology of PDGFR::mCherry electroporated cell. Color code indicates depth relative to ventricular surface. (**D**) Coronal sections showing PDGFRβ immunostaining in quiescent (orange arrowhead) and some activated (white arrowhead) NSCs but not in TACs (asterisks). V, ventricle. (**E** and **F**) Lineage-tracing of PDGFRβ^{+} cells showing GFP^{+} new neurons in the OB (E) and radial stem cells in V-SVZ (F) (arrowheads) at 120 dpi. (**G**) Representative FACS multigraph overlay showing distribution of PDGFRβ^{+} cells in purified GFAP::GFP^{+}CD24^{-} subpopulations gated on EGFR and CD133. (**H**) Activation kinetics of FACS-purified populations in vitro; n = 5 experiments. d0, day 0. (**I**) Genome-wide correlation analysis of gene expression profiles. CX, cortex. Scale bars, 10 μm.

hotspot in the dorsoseptal corner (Fig. 3, F and G, and fig. S5, F and H). These septal Olig2$^+$ domains were already present during development at postnatal days 1 and 10 (fig. S5, I and J). In addition to the dorsolateral wedge, another oligodendrogenic domain was present in the lateral wall at more-caudal levels (fig. S5F). Our single-cell transcriptional profiling indicated that the septal wall is more oligodendrogenic than the lateral wall (*16*). We therefore compared the differentiation potential of FACS-purified PDGFRβ$^+$GFAP::GFP$^+$ adult NSCs from both walls of adult wild-type mice, which directly showed that septal NSCs gave rise to more O4$^+$ oligodendrocytes and fewer TuJ1$^+$ neurons than did lateral NSCs (fig. S5, K and L).

The above gliogenic domains are largely quiescent under homeostasis. To investigate whether they respond to injury in wild-type mice, we performed focal demyelination in the corpus callosum by unilateral injection of lysolecithin (fig. S6, A and B). At 2 dpi, dividing MCM2$^+$ cells increased around the ipsilateral ventricle (fig. S6C). More radial stem cells were recruited to divide in both the septal and lateral walls (fig. S6, D and F). Olig2$^+$MCM2$^+$ cells were increased in all domains at 2 dpi (Fig. 3, H and I, and fig. S6J) but became restricted to septal domains at 5 dpi (fig. S6, K and L). Gorditas were also increased in lysolecithin-injected mice, and many were MCM2$^+$ (Fig. 3, J and K, and fig. S6, G to I). Thus, these more quiescent gliogenic domains, as well as gorditas, are recruited in response to physiological demand.

Unexpectedly, we also identified an unknown PDGFRα$^+$ cell type inside the brain ventricles, which we call intraventricular oligodendrocyte progenitors (OPCs). In PDGFRβ$^\Delta$ mice, numerous intraventricular Tom$^+$Olig2$^+$ cells derived from GFAP$^+$ NSCs were attached to the luminal surface of the wall (Fig. 4A). Intraventricular OPCs were also present in wild-type brains, which we characterized further. Their morphology and distribution were most clearly visualized in whole-mount preparations. Intraventricular OPCs were localized on top of ependymal cells nestled between their cilia (Fig. 4, B and C), in the rostral portion of both the lateral and septal walls of the ventricle (fig. S7, A, B, and E). They expressed typical OPC markers (Olig2$^+$, NG2$^+$, and PDGFRα$^+$) (Fig. 4, B to D, and fig. S7F) and frequently contacted each other (fig. S7, A and B). Lineage tracing and immunostaining showed that intraventricular OPCs arose from tight clusters of GFAP$^+$PDGFRβ$^+$ cells (Fig. 4D), which gave rise to PDGFRα$^+$ cells, some of which retained GFAP, that then dispersed as individual PDGFRα$^+$-only cells, with an increasingly ramified morphology (fig. S7, C, G, H, and J). Intraventricular OPCs differed morphologically from PDGFRα$^+$ OPCs found in the SVZ and brain parenchyma (Fig. 4B and fig. S7, C and D). Unlike parenchymal OPCs, they expressed EGFR in the nucleus, and many were Ascl1$^+$ (fig. S7, K and L). Some were dividing on the basis of MCM2 and Ki67 expression (fig. S7, M to O). Intraventricular OPCs first appeared around postnatal days 5 and 7 (fig. S8A), paralleling an increase in PDGFAA ligand in the choroid plexus (fig. S8B), and increased in number to 2 months. Their number decreased over time, and at 14 months, clusters—but few dispersed cells—were still present (fig. S8A). After focal demyelination with LPC, intraventricular OPCs initially disappeared at 2 dpi but then increased in number at 5 dpi (fig. S8, C to G).

Many intraventricular OPCs were closely apposed to or partially enwrapped supraependymal axons present on the surface of both walls of the lateral ventricles, including serotonergic axons (Fig. 4, E and F, and fig. S8H) that regulate NSC proliferation (*17*). We did not detect mature myelinating Rip, myelin oligodendrocyte glycoprotein (MOG), or myelin basic protein (MBP)$^+$ oligodendrocytes inside the ventricles (fig. S7, P to R), suggesting that intraventricular OPCs do not give rise to myelinating oligodendrocytes in situ. Given their location,

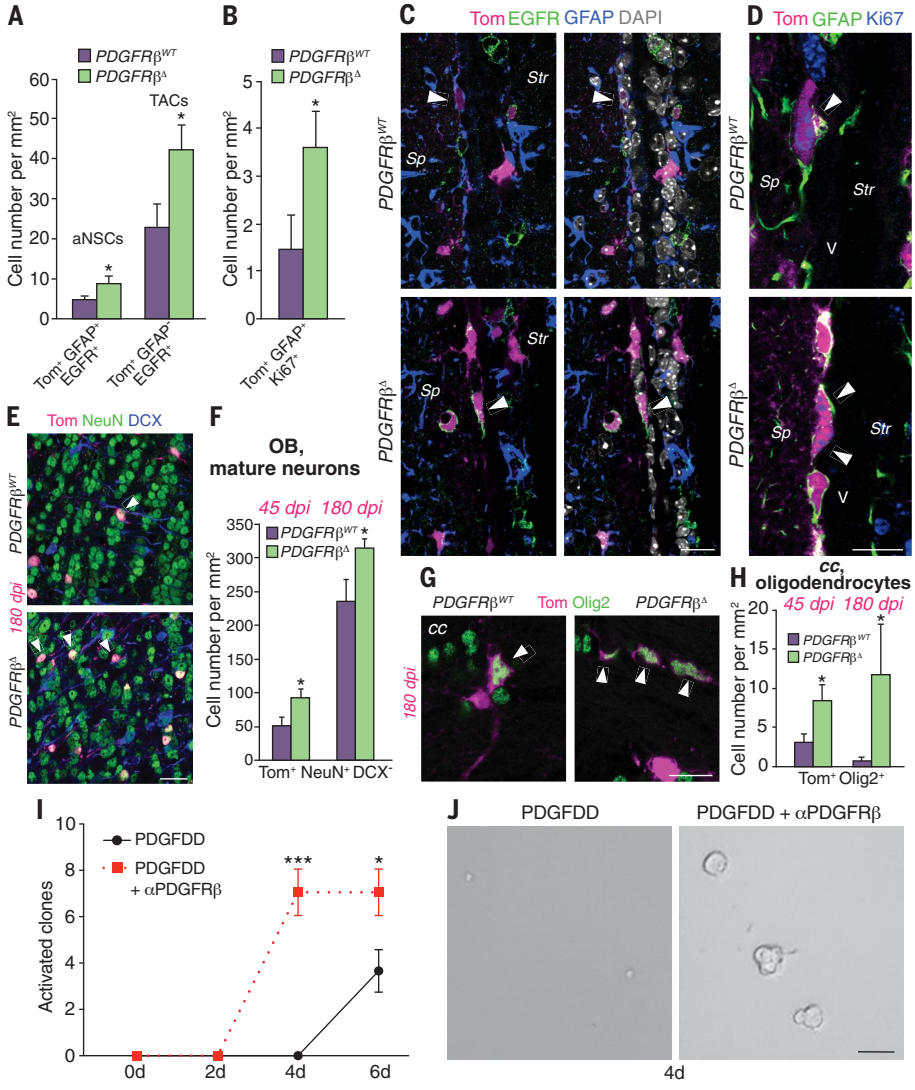

Fig. 2. PDGFRβ deletion releases adult NSCs from quiescence. (**A**) Quantification of Tom$^+$ aNSCs, TACs, and (**B**) GFAP$^+$ dividing cells at 1 dpi in PDGFRβ^{WT} and PDGFRβ$^\Delta$ mice; *n* = 4 mice per group. (**C**) Immunostaining of V-SVZ coronal sections showing Tom$^+$ aNSCs and (**D**) dividing GFAP$^+$ cells at 1 dpi (arrowheads). Tom, tdTomato; DAPI, 4′,6-diamidino-2-phenylindole. (**E**) Images of Tom$^+$NeuN$^+$ neurons in the olfactory bulb (OB) and (**F**) quantification at 45 and 180 dpi; *n* = 4 mice per group. (**G**) Tom$^+$Olig2$^+$ cells (arrowheads) in the corpus callosum (cc) and quantification (**H**) at 45 and 180 dpi; *n* = 4 mice per group. (**I**) Time course of activation and (**J**) images of Pβ$^+$CD133$^+$ qNSCs treated with PDGFDD or PDGFDD and αPDGFRβ; *n* = 5 experiments. Scale bars, 10 μm. *P < 0.05, ***P < 0.001. Error bars indicate SEM.

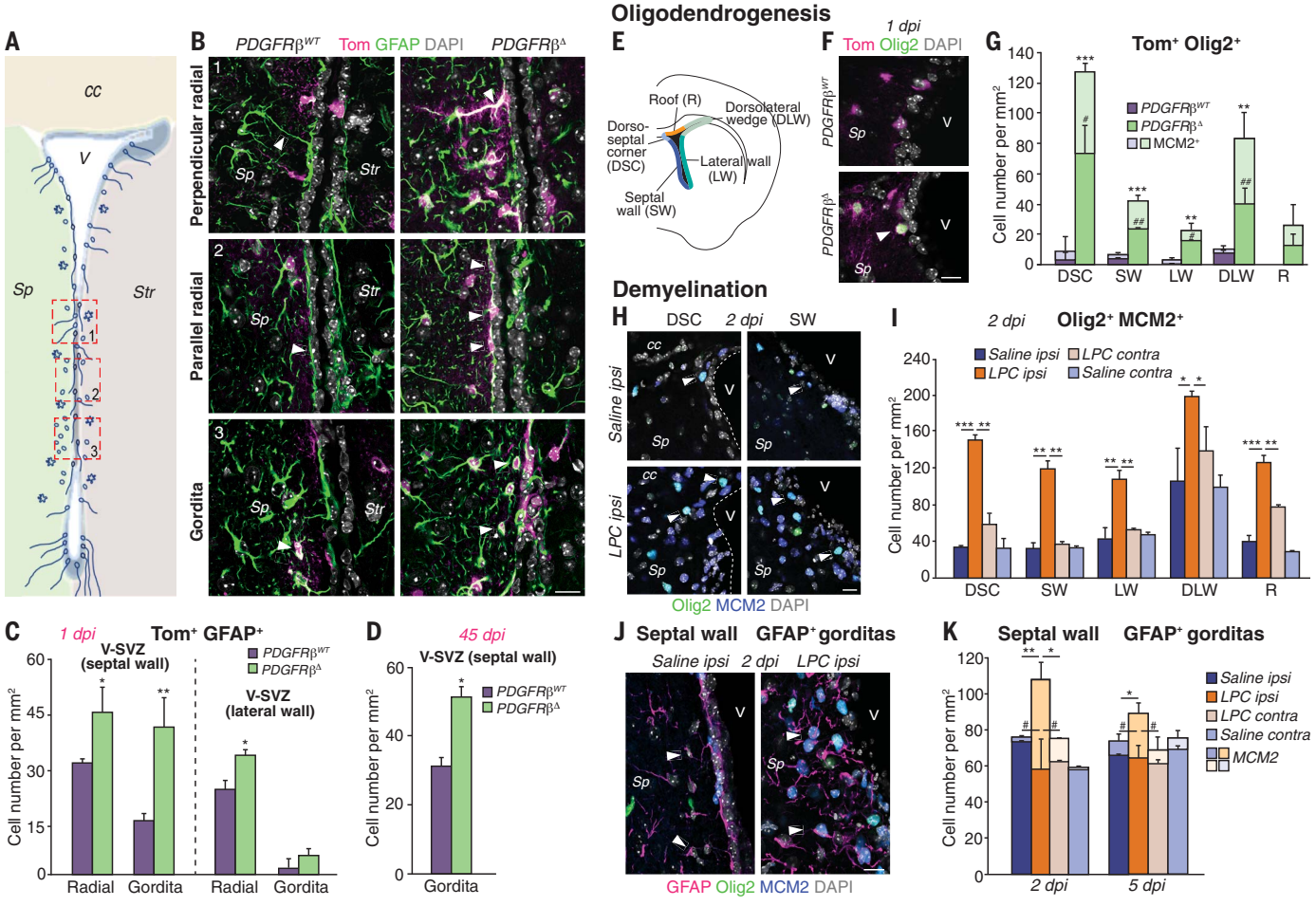

Fig. 3. Gliogenic domains in the adult V-SVZ. (**A**) Coronal schema depicting distribution of different types of GFAP$^+$ cells in adult V-SVZ. Boxes and numbers show location of images in (B). (**B**) Different types of Tom$^+$GFAP$^+$ cells (arrowheads) at 1 dpi. (**C**) Quantification of radial cells and gorditas in the lateral and septal walls at 1 dpi; *n* = 4 mice per group. (**D**) Quantification of gorditas in the septal wall at 45 dpi; *n* = 4 mice per group. (**E** to **G**) Oligodendrogenic domains. (E) Coronal schema showing domains analyzed in the V-SVZ. (F) Tom$^+$Olig2$^+$ cells (arrowhead) in the dorsoseptal corner of V-SVZ. (G) Quantification of Tom$^+$Olig2$^+$ cells in different domains of V-SVZ from Bregma +1.2 to 0 mm in PDGFRβ^{WT} and PDGFRβ$^{\Delta}$ mice; *n* = 4 mice per group. (**H** to **K**) Demyelination. (H) Images of Olig2$^+$MCM2$^+$ cells (arrowheads) and (I) quantification in different V-SVZ domains at 2 dpi; *n* = 3 mice per group. LPC, lysolecithin. (J) Images of gorditas (arrowheads) in the septal wall at 2 dpi and (K) their quantification at 2 and 5 dpi; *n* = 3 mice per group. Scale bars, 10 μm. $^*P < 0.05$, $^{**}P < 0.01$, $^{***}P < 0.001$. $^{\#}P < 0.05$, $^{\#\#}P < 0.01$ (MCM2 comparisons). Error bars indicate SEM.

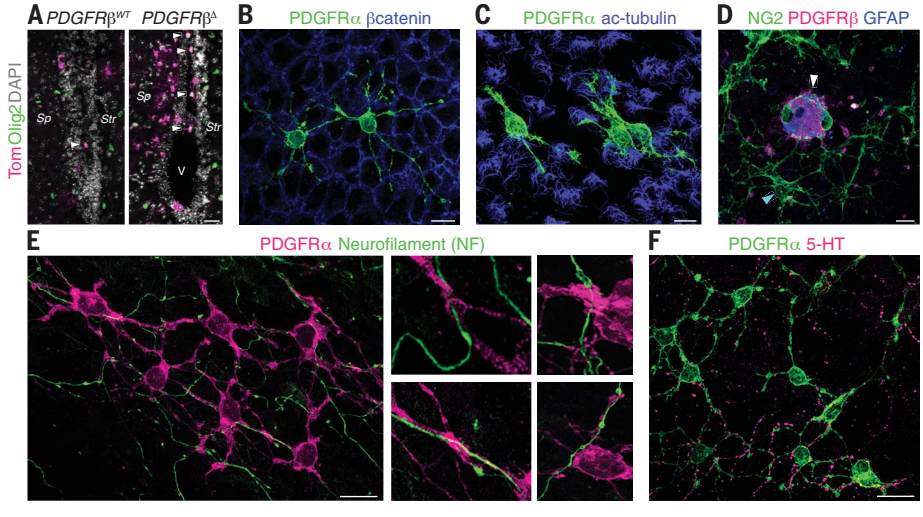

Fig. 4. Intraventricular oligodendrocyte progenitors. (**A**) Tom$^+$Olig2$^+$ intraventricular OPCs in coronal sections of PDGFRβ^{WT} and PDGFRβ$^{\Delta}$ mice. (**B** to **F**) Whole-mount immunostaining of intraventricular OPCs in wild-type mice. (B) PDGFRα$^+$ OPCs on ventricular surface (β-catenin) and (C) among the cilia of ependymal cells (ac-tubulin). (D) PDGFRβ$^+$GFAP$^+$NG2$^+$ cluster (white arrowhead) and dispersed NG2$^+$ OPCs that are PDGFRβ$^-$ (blue arrowhead). [(E) and (F)] Association of intraventricular OPCs with supraependymal Neurofilament$^+$ (E) and serotonergic (5-HT) (F) axons. Scale bars, 10 μm.

intraventricular OPCs are poised to integrate and dynamically respond to signals from the cerebrospinal fluid and diverse cell types, including axons from other brain regions.

Here, we uncover multiple gliogenic domains in the adult V-SVZ that are more quiescent under homeostasis and are recruited in response to focal injury. Stem cells in these spatially distinct domains may be differentially recruited in different physiological states, as occurs for olfactory bulb neuron subtypes (*18*), to generate specific glial subtypes in a context-dependent manner. The identification of two unknown glial cell types in the adult brain further highlights the extent of glial diversity and opens vistas into understanding the role of neural stem cells and glia in health and disease.

REFERENCES AND NOTES

1. Z. Chaker, P. Codega, F. Doetsch, *Wiley Interdiscip. Rev. Dev. Biol.* **5**, 640–658 (2016).
2. P. Codega *et al*., *Neuron* **82**, 545–559 (2014).
3. F. Doetsch, I. Caillé, D. A. Lim, J. M. García-Verdugo, A. Alvarez-Buylla, *Cell* **97**, 703–716 (1999).
4. Z. Mirzadeh, F. T. Merkle, M. Soriano-Navarro, J. M. Garcia-Verdugo, A. Alvarez-Buylla, *Cell Stem Cell* **3**, 265–278 (2008).
5. F. Doetsch, J. M. García-Verdugo, A. Alvarez-Buylla, *Proc. Natl. Acad. Sci. U.S.A.* **96**, 11619–11624 (1999).
6. M. Vanlandewijck *et al*., *Nature* **554**, 475–480 (2018).
7. E. Llorens-Bobadilla *et al*., *Cell Stem Cell* **17**, 329–340 (2015).
8. J. Schmahl, K. Rizzolo, P. Soriano, *Genes Dev.* **22**, 3255–3267 (2008).
9. Y. Ishii *et al*., *J. Neurochem.* **98**, 588–600 (2006).
10. V. Silva-Vargas, A. R. Maldonado-Soto, D. Mizrak, P. Codega, F. Doetsch, *Cell Stem Cell* **19**, 643–652 (2016).
11. Y. Ishii *et al*., *Mol. Cell. Neurosci.* **37**, 507–518 (2008).
12. G. Xu *et al*., *Neuroscience* **238**, 195–208 (2013).
13. A. Armulik *et al*., *Nature* **468**, 557–561 (2010).
14. R. Daneman, L. Zhou, A. A. Kebede, B. A. Barres, *Nature* **468**, 562–566 (2010).
15. K. Azim, B. Berninger, O. Raineteau, *Front. Neurosci.* **10**, 107 (2016).
16. D. Mizrak *et al*., *Cell Rep.* **26**, 394–406.e5 (2019).
17. C. K. Tong *et al*., *Cell Stem Cell* **14**, 500–511 (2014).
18. A. Paul, Z. Chaker, F. Doetsch, *Science* **356**, 1383–1386 (2017).

ACKNOWLEDGMENTS

We thank members of the Doetsch and Wichterle labs and D. Thaler for discussion; V. Crotet for genotyping; the Biozentrum Imaging Core Facility; K. Gordon and S. Tetteh of the Herbert Irving Comprehensive Cancer Center Flow Cytometry Core of Columbia University for assistance with FACS; and J. Bögli at the Biozentrum FACS Core Facility. **Funding:** This work was supported by NIH NINDS R01 NS074039, Swiss National Science Foundation 31003A_163088, and European Research Council Advanced Grant 789328 (F.D.); University of Basel, NINDS grant 1F31NS079057 (A.R.M.-S.); NRSA Ruth Kirschstein Postdoctoral Fellowship NINDS F32 NS090736 (D.M.); Swiss National Science Foundation BSSGIO_155830 (K.R.T.); NINDS F31NS089252 (A.P.); NIH NHLBI R01 HL112626 (J.K.); and NCI 5P30CA013696 (C.-S.L). **Author contributions:** Conceptualization: F.D., A.R.M.-S., and A.C.D. Performed experiments: A.C.D., A.R.M.-S., V.S.-V., D.M., T.v.K., K.R.T., A.P., and H.C. Data analysis: A.C.D., A.R.M.-S., V.S.-V., D.M., and A.M. Supervision: F.D. Manuscript writing: A.C.D., A.R.M.-S., V.S.-V., D.M., and F.D. Resources: H.C., J.K., and C.-S.L contributed PDGFRβ-P2A-CreER^{T2};mT/mG mice. **Competing interests:** The authors declare no competing interests. **Data and materials availability:** RNA-seq data of the FACS-purified populations are deposited in the National Center for Biotechnology Information Gene Expression Omnibus under accession number GSE118009. All other data are in the main paper or supplementary materials.

SUPPLEMENTARY MATERIALS

science.sciencemag.org/content/372/6547/1205/suppl/DC1
Materials and Methods
Figs. S1 to S8
Tables S1 to S3
References (*19*–*30*)
MDAR Reproducibility Checklist

View/request a protocol for this paper from *Bio-protocol*.

3 February 2021; accepted 16 April 2021
10.1126/science.abg8467

Release of stem cells from quiescence reveals gliogenic domains in the adult mouse brain

Ana C. Delgado, Angel R. Maldonado-Soto, Violeta Silva-Vargas, Dogukan Mizrak, Thomas von Känel, Kelly R. Tan, Alex Paul, Aviv Madar, Henar Cuervo, Jan Kitajewski, Chyuan-Sheng Lin, and Fiona Doetsch

Science **372** (6547), . DOI: 10.1126/science.abg8467

Gliogenesis in the adult mouse brain

Neural stem cells in the adult mouse brain can generate both neurons and glia. Exactly where each stem cell is positioned can determine what type of neurons it generates. Delgado *et al.* show that neural stem cells are also choosy about what sorts of glia they make and when (see the Perspective by Baldwin and Silver). Injury or selective deletion of platelet-derived growth factor receptor # (PDGFR#) from the stem cells kicked them into overdrive and revealed their selectivity with respect to gliogenesis. An unusual type of glial progenitor cell, intraventricular oligodendrocyte progenitors, are found nestled between the cilia of ependymal cells derived from tight clusters of PDGFR#-expressing stem cells.

Science, abg8467, this issue p. 1205; see also abj1139, p. 1151